Fatigue assessment of a FSAE car rear upright by a closed form solution of the critical plane method

A.Chiocca*, M. Sgamma, F. Frendo, F. Bucchi
Department of Civil and Industrial Engineering, University of Pisa, Pisa, Italy
andrea.chiocca@unipi.it, http://orcid.org/0000-0002-1472-4398
michele.sgamma@phd.unipi.it, https://orcid.org/0009-0003-8637-9946
francesco.frendo@unipi.it, http://orcid.org/0000-0002-7472-4664
francesco.bucchi@unipi.it, http://orcid.org/0000-0001-7840-3158

G. Marulo
Pierburg Pump Technology Italy S.p.A., Livorno, Italy
giuseppe.marulo@it.rheinmetall.com

Citation: Chiocca A. Sgamma, M., Frendo, F., Bucchi, F., Marulo, G., Fatigue assessment of a FSAE car rear upright by a closed form solution of the critical plane method, Frattura ed Integrità Strutturale, 67 (2024) 153-162.

Received: 20.10.2024
Accepted: 24.11.2024
Online first: 26.11.2023
Published: 01.01.2024

KEYWORDS. Critical plane; Multiaxial fatigue; Fatigue evaluation; Computational efficiency; Finite element analysis; Lightweight design.

INTRODUCTION

The topic of material fatigue holds significant importance within both the scientific and industrial communities ([1]–[4]). The majority of component failures during service can be attributed to fatigue failure ([5]–[7]), presenting a major design challenge due to the complexities associated with real-world applications, including variable amplitude, randomness, multiaxiality and residual stresses ([8]–[13]).

Currently, the automotive industry is witnessing a growing trend towards the utilization of innovative materials and lightweight design. This trend aims to reduce overall environmental impact and promote human health. Consequently, there is an increased demand for efficient and accurate design tools.

Finite element analysis (FEA) has become a standard methodology for accounting for the complexities of component geometries and applying appropriate load histories ([14]–[18]). However, simulations can be time-consuming, particularly during the post-processing phase, where various methods can be employed. The numerous approaches to assess damage can be categorized into a few groups, typically categorized as energy-based or stress/strain-based methods. Energy-based approaches (both elastic and plastic) exist to describe the fatigue behavior of notched and unnotched components under multiaxial loading conditions ([19]–[26]). Whereas, strain-based methods are typically used to investigate low-cycle fatigue scenarios, while stress-based approaches are typically employed in high-cycle fatigue scenarios ([27]–[30]).

A specific category of methods is based on the critical plane (CP) concept. This approach is a local method that involves evaluating a given CP factor in every possible orientation at any given location within the model. Consequently, the point and plane orientation experiencing the highest CP value, known as the critical plane factor, are determined ([31]–[34]). The critical plane factor plays a crucial role in fatigue life prediction of components by quantifying the material's ability to endure fatigue under complex loading conditions. However, implementing the CP method can be time-consuming, especially for three-dimensional models with complex geometries. It requires scanning numerous planes in three-dimensional space using nested *for/end* loops. Sometimes, the iterative process is further slowed down as unnecessary quantities are evaluated on each rotated plane. Since defining the critical region in advance is not always possible, the implementation process may need to be applied to every node in the model particularly for models with intricate geometries, load histories, and constraints. In this context, the utilization of optimization algorithms or analytical formulations can be beneficial for enabling a comprehensive analysis of the component. Efforts have been made to reduce the computational time required for critical plane factor calculations. Previous research explored methods leveraging analytical or semi-analytical techniques to determine the damage factor and its maximized direction. The studies authored by Chiocca and colleagues ([35], [36]) introduce diverse computational algorithms designed to optimize the computation of critical plane models, including renowned models like the *Fatemi-Socie*, *Smith-Watson-Topper*, and *Kandil-Brown-Miller* criteria. These algorithms employ closed-form expressions to calculate specific critical plane factors and the associated orientations of critical planes. Marques et al. [37] introduced an algorithm focusing on calculating the spectral parameters related to the damage factor using analytical formulas. Other approaches aimed at enhancing the computational speed by selectively calculating the critical plane factor in specific planes rather than exhaustively scanning the entire space. Wentingmann et al. [38] developed an algorithm that accelerated critical plane detection by segmenting a coarse Weber half sphere with quad elements. Similarly, Sunde et al. [39] devised an adaptive scheme that densified a triangular mesh around elements where the greatest damage had been observed. These advancements have shown promise in reducing computation time, thereby enabling more efficient fatigue assessment procedures.

This paper presents a rapid and accurate procedure for fatigue assessment applied to a Formula SAE racing car rear upright. The procedure is based on a closed-form solution of the critical plane factor recently introduced by Chiocca et al. [35]. The procedure is applied in the case of elastic-plastic material behaviour, multiaxiality and non-proportional loading conditions. The component under study undergoes a load cycle comprising two different on-track conditions: right-turn with braking and right-turn with acceleration. The component's geometry and applied loads are derived from previous dynamic analysis and topological optimization studies conducted by the University of Pisa's Formula SAE team.

STANDARD PLANE SCANNING METHOD

The scanning plane technique (Fig. 1) involves defining a plane (Γ) with its unit normal vector ($\boldsymbol{n}$) and incrementally rotating the plane by fixed angular steps along different directions (typically two angles, e.g., θ and ψ with angular increments $\Delta\theta$ and $\Delta\psi$). This enables precise evaluation of stresses and strains in all possible orientations in space. This approach is a sort of *blind search-for* method, which inherently suffers from inefficiency as it necessitates scanning through all conceivable planes to identify the one where a given fatigue parameter reaches its maximum value. In order to apply this method, nested *for/end* loops have to be implemented in a general-purpose program, resulting in extended computation times for each individual node.

For this study, a rotational sequence was used within a moving frame of reference. The sequence comprised an initial rotation by an angle ψ about the z-axis, followed by a rotation θ about the y-axis. This sequence is presented in Eqn. 1:

$$R = R_z(\psi)R_y(\theta) = \begin{pmatrix} \cos(\theta)\cos(\psi) & -\sin(\psi) & \sin(\theta)\cos(\psi) \\ \cos(\theta)\sin(\psi) & \cos(\psi) & \sin(\theta)\sin(\psi) \\ -\sin(\theta) & 0 & \cos(\theta) \end{pmatrix} \quad (1)$$

To carry out the scanning procedure, an angular increment of 1° was employed for both $\Delta\theta$ and $\Delta\psi$.

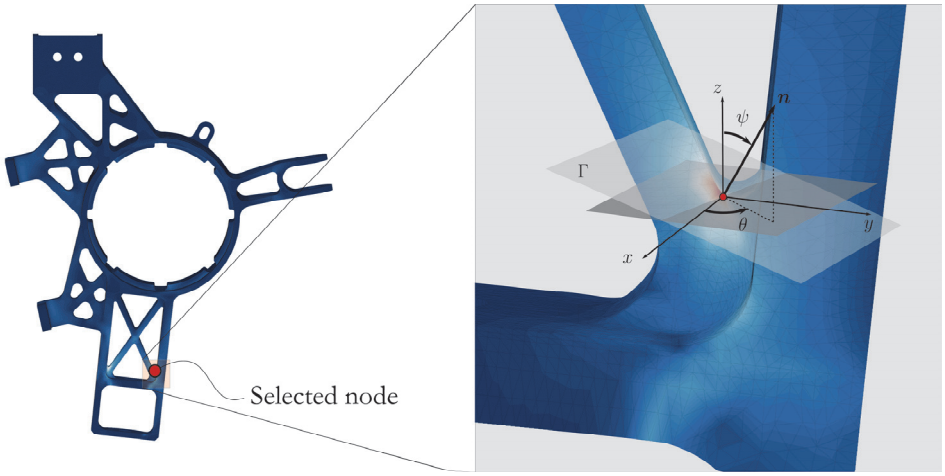

Figure 1: Standard plane scanning method applied to the critical node of a generic finite element component.

CRITICAL PLANE FACTORS EVALUATION BY MEANS OF THE EFFICIENT METHOD

The method will be presented with reference to two reference critical plane factors, chosen to reflect different material damage processes (i.e., shear-cracking and tensile-cracking):

– the *Fatemi-Socie* critical plane factor [40], denoted as ***FS*** in Eqn. 2:

$$FS = \frac{\Delta\gamma_{max}}{2}\left(1 + k\frac{\sigma_{n,max}}{\sigma_y}\right) = \frac{\tau'_f}{G}\left(2N_f\right)^{b_0} + \gamma'_f\left(2N_f\right)^{c_0} \quad (2)$$

the material parameter k is determined by fitting the uniaxial experimental data against the pure torsion data; in this equation, $\Delta\gamma_{max}$ represents the maximum shear strain range, $\sigma_{n,max}$ denotes the maximum normal stress acting on the plane experiencing $\Delta\gamma_{max}$, and σ_y represents the material's yield strength. This critical plane model is commonly employed for materials prone to shear cracking; the right-hand side of Eqn. 2 corresponds to the shear strain-life curve specific to the material under investigation; the material parameters utilized to define the shear strain-life curve can be found in Tab. 1, taken from Gates and Fatemi [41];

– the *Smith-Watson-Topper* critical plane factor that includes Socie's modification [30], denoted as ***SWT*** in Eqn. 3:

$$SWT = \frac{\Delta\varepsilon}{2}\sigma_{n,max} = \frac{\sigma'^2_f}{E}\left(2N_f\right)^{2b} + \sigma'_f\varepsilon'_f\left(2N_f\right)^{b+c} \quad (3)$$

where $\frac{\Delta\varepsilon}{2}$ represents the maximum strain amplitude, while $\sigma_{n,max}$ indicates the maximum normal stress acting on the plane identified by $\frac{\Delta\varepsilon}{2}$; this critical plane model is commonly utilized for materials prone to tensile cracking, as opposed to the ***FS*** model; the right-hand side of Eqn. 3 represents the uniaxial strain-life curve specific to the material being

studied; the material parameters necessary to define the uniaxial strain-life curve can be found in Tab. 1, taken from Gates and Fatemi [41].

The evaluation of the two critical plane factors will be conducted utilizing the analytical formulation proposed by Chiocca et al. [35], which highly speeds up the calculation of CP factor for each node, since it does not requires to scan all possible orientations at any given point. The analytical solution is derived from tensor invariants and coordinate transformation laws. A graphical representation of the method is depicted in Fig. 2 in the case of *Fatemi-Socie* CP factor. Fig. 2 reports the three main steps involved in the method. The first step consists in determining the stress-strain range tensors representing the fatigue cycle on the basis of the stress and/or strain results obtained from a FE-simulation of the given load conditions; by considering the stress and strain range tensor, the second step involves an *eigenvalue/eigenvector* analysis (i.e., $\boldsymbol{\Delta\sigma}$ or $\boldsymbol{\Delta\varepsilon}$ depending on the CP method taken as reference) in order to obtain the principal components, which can be conveniently reported on the circular representation, allowing an easy identification of the maximum stress or the maximum strain range; finally, in the third step the strain range tensor is rotated by an angle ω around the median principal axis ($\boldsymbol{n}_2$) in order to obtain the critical plane. Notably, the angle ω varies depending on the CP method adopted; for the *FS* method, $\omega = \frac{\pi}{4}$, whereas for the *SWT* method, $\omega = 0$.

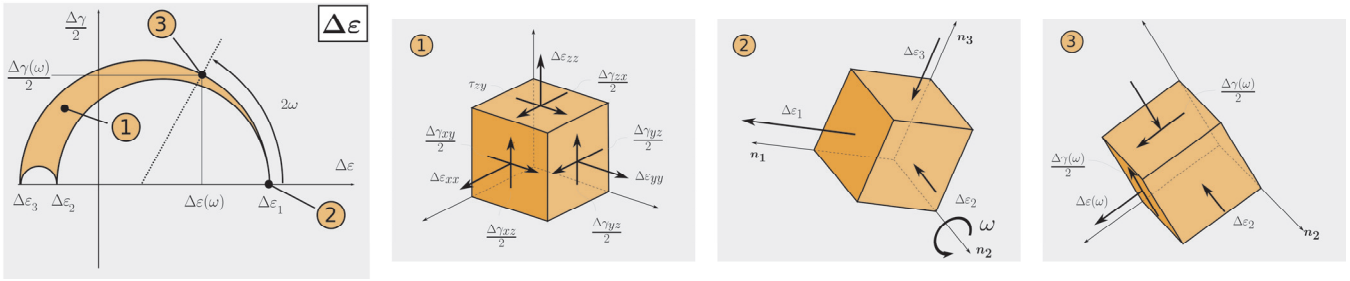

Figure 2: Standard plane scanning method applied to a node of a generic finite element component.

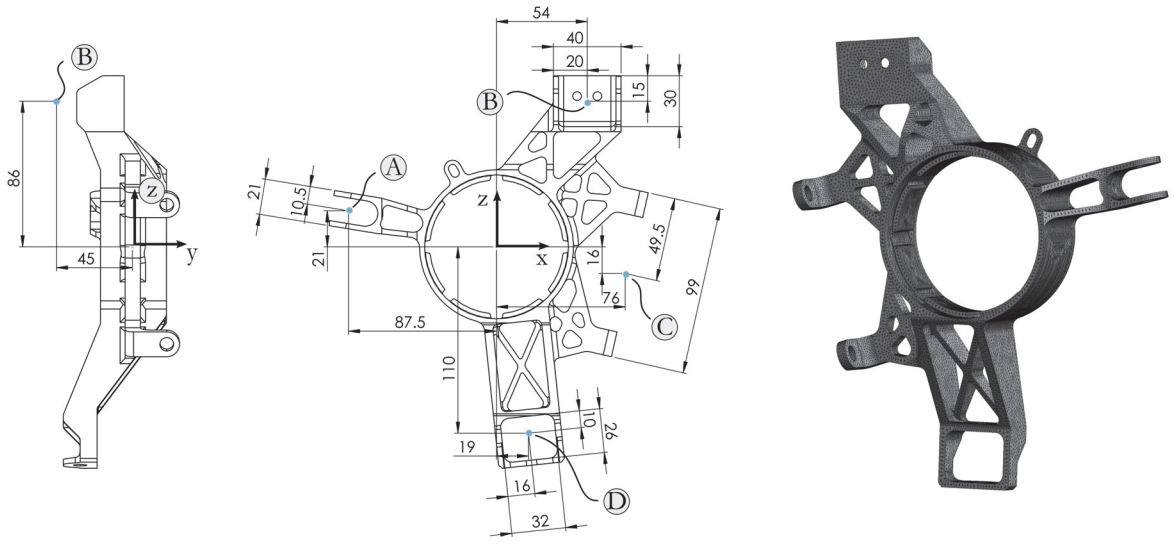

(a) (b)

Figure 3: Upright component: (a) technical drawing with indicated the position of load application points and (b) the corresponding meshed structure.

MATERIAL AND METHODS

The focus of this study is the examination of a rear upright for a Formula SAE (FSAE) car, as illustrated in Fig. 3. An upright is part of the wheel assembly, enabling the transfer of loads from the wheel to the suspension system. The component in question was fabricated through CNC machining using a single piece of 7075-T6 aluminium, with its

properties detailed in Tab. 1. As it can be seen, the component exhibits a complex geometry, featuring several potential critical notches where fatigue cracks may initiate. Fig. 3 additionally indicates the position, with respect to the wheel axis, of the load application points, used in the following FE-analysis.

Shear fatigue properties			
S.f. strength coefficient (τ'_f)	S.f. strength exponent (b_0)	S.f. ductility coefficient (γ'_f)	S.f. ductility exponent (c_0)
797 MPa	-0.126	5.42	-1.173
Uniaxial fatigue properties			
F. strength coefficient (σ'_f)	F. strength exponent (b)	F. ductility coefficient (ε'_f)	F. ductility exponent (c)
1235 MPa	-0.138	0.243	-0.710
Monotonic properties			
0.2% Yield strength (σ_y)	Young's modulus (E)	Elastic Poisson's ratio (ν)	Ultimate tensile strength (σ_u)
501 MPa	71.7 GPa	0.306	561 MPa
Cyclic deformation properties			
0.2% Cyclic axial strength (σ'_y)	Cyclic strength coefficient (K')		Cyclic axial hardening exponent (n')
518 MPa	845 GPa		0.079

Table 1: Material properties of 7075-T6 aluminium obtained from Gates and Fatemi [41] (i.e., *S.f.* stands for *Shear fatigue* and *F.* stands for *Fatigue*).

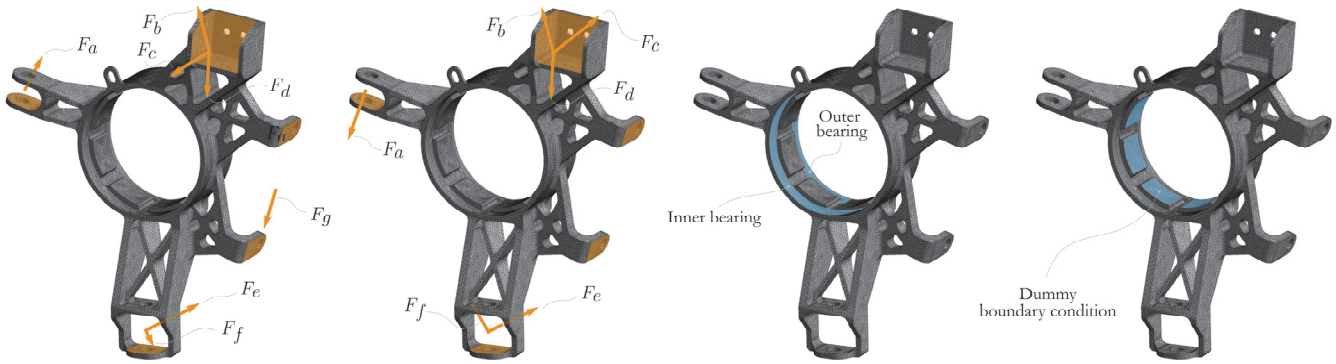

Figure 4: Applied boundary conditions during the FE-analysis; the orange arrows and orange surfaces represent the applied loadings (a) for load step n. 1 and (b) for the load step n. 2, while the blue surfaces represent the displacement constraints, (c) bearing constraint and (d) dummy rotational constraint.

For the finite element analysis loading conditions derived from a prior numerical dynamic study were employed; the analysis was conducted by the SAE formula racing team at the University of Pisa during the 2020 season. Specifically, the loads are derived from a rear suspension analysis of a single-seater car, with rear-wheel drive, fitted with a Honda 600 engine that develops a peak torque of 60 Nm at 9000 rpm and allows 0-100 Km/h acceleration in 3.5s. To perform the finite element analysis the Ansys Workbench software was employed. The applied loading conditions, illustrated in Fig. 4, encompass two loading steps corresponding to particularly demanding cornering scenarios. The first load condition (load step n. 1, Fig. 4a) simulates a right-turn with braking, while the second load condition (load step n. 2, Fig. 4b) replicates a right-turn with acceleration. In both cases, *remote forces* were applied in the orange highlighted areas, whose absolute value and direction are shown in Tab. 2, by using the remote points (i.e., A, B, C and D) shown in Fig. 4. Additionally, *remote displacement* constraints were applied to represent the upright bearings (Fig. 4c), while a dummy *remote displacement* was introduced to prevent rotational instability (Fig. 4d). Post-processing analysis confirmed that the reaction on the dummy constraint was indeed zero.

The applied loading condition exhibits constant amplitude and non-proportionality. As a matter of fact, as shown in Fig. 5a, the time evolution of the equivalent force at points A, B, C and D can be described by means of only two load steps.

The resulting stress and strain history is non-proportional as demonstrated in Fig. 5b by the change in the principal stress reference frame between load step n.1 and n.2 at the critical node (i.e. whose position was found during the analysis presented in the next section).

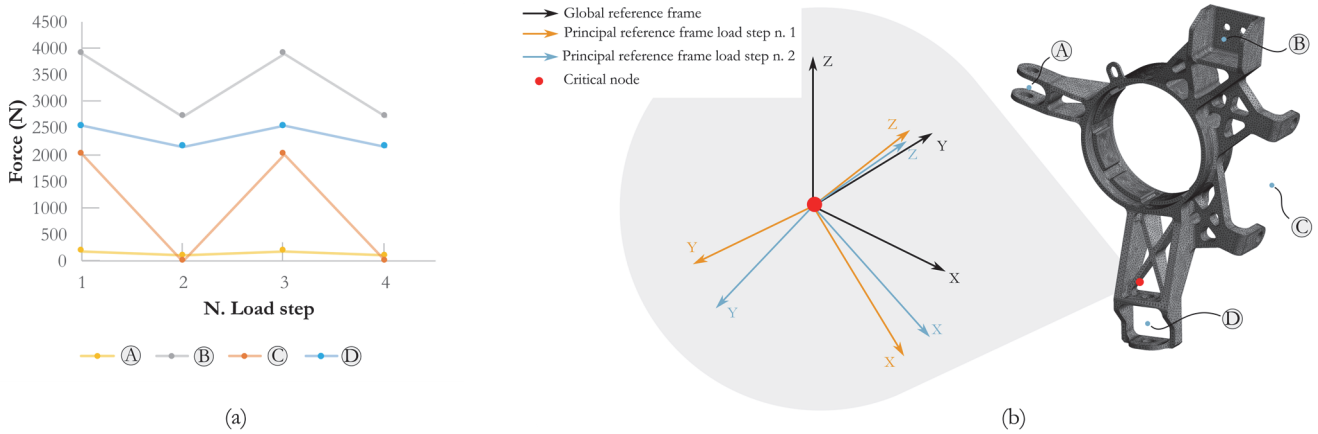

(a) (b)

Figure 5: Equivalent forces applied at points A, B, C and D over the load steps (a) and comparison of the principal reference frames between the two loading conditions (b).

The finite element model employed stabilized elastic-plastic material properties, as outlined in Tab. 1. The cyclic properties of the material were implemented through the material parameters K', n' and σ'_y, while the linear-elastic part was modelled by means of E and ν. A multilinear kinematic hardening law was implemented, utilizing a discrete sampling of the Ramberg-Osgood law presented in Eqn. 4.

$$\varepsilon_{tot} = \left(\frac{\sigma}{E}\right) + \left(\frac{\sigma}{K'}\right)^{\frac{1}{n'}} = \varepsilon_{el} + \varepsilon_{pl} \tag{4}$$

Load step	F_a (N)	F_b (N)	F_c (N)	F_d (N)	F_e (N)	F_f (N)	F_g (N)
n. 1	180.5	1828	675	1600	1693	1288	2008
n. 2	104	666	430	1774	42	2151	0
A		B		C		D	
$F_a \rightarrow (-0.24, 0.93, 0.25)$		$F_b \rightarrow (-0.65, 0.70, 0.27)$ $F_c \rightarrow (-0.16, 0.91, 0.35)$ $F_d \rightarrow (-0.45, 0.59, 0.66)$		$F_g \rightarrow (-0.22, 0, -0.97)$		$F_f \rightarrow (-0.72, 0.68, 0.01)$ $F_e \rightarrow (0.20, 0.97, 0.09)$	

Table 2: Absolute values of applied forces and their directional versors (with reference to the global reference frame Oxyz of Fig. 3) during the finite element simulation.

RESULTS AND DISCUSSION

Based on the finite element analysis, stress and strain data can be extracted for each node and load step. This allows for the calculation of critical plane factors, as presented in Eqns. 2-3. It should be noted that the critical plane method provides the damage calculated for a single fatigue loading cycle, corresponding to a load step pair in the finite element analysis. In this case, due to the geometric complexity of the component and the non-proportional loading sequence applied, identifying the critical region in advance is not possible and an overall assessment of the entire component becomes necessary. Employing the conventional plane scanning method to calculate the damage factor for the entire model, which consists of 61367 nodes, takes about 7.3 hours on an 11th Gen Intel(R) Core(TM) i7 with 16GB of available RAM and 4 cores, considering 1° of angular step. In contrast, by using the previously shown closed form solution directly in Ansys

Workbench, the desired results can be obtained much faster, within 63 s, significantly simplifying the fatigue assessment of the whole part. Fig. 6 shows the computational cost required to calculate the CP factor for a single node in the case of the standard plane scanning method and the closed form solution. It is worth noting that the time required to evaluate the closed-form solution does not depend on the defined angular step since it is based on an analytical formulation, which does not require to scan different orientations. In addition, the closed-form formulation would enable further code speed-up by utilizing lower-level programming languages. As a matter of fact, the limitation is mainly given by the programming execution speed since it is no longer dependent by nested *for/end* loops as in the case of the standard plane scanning method.

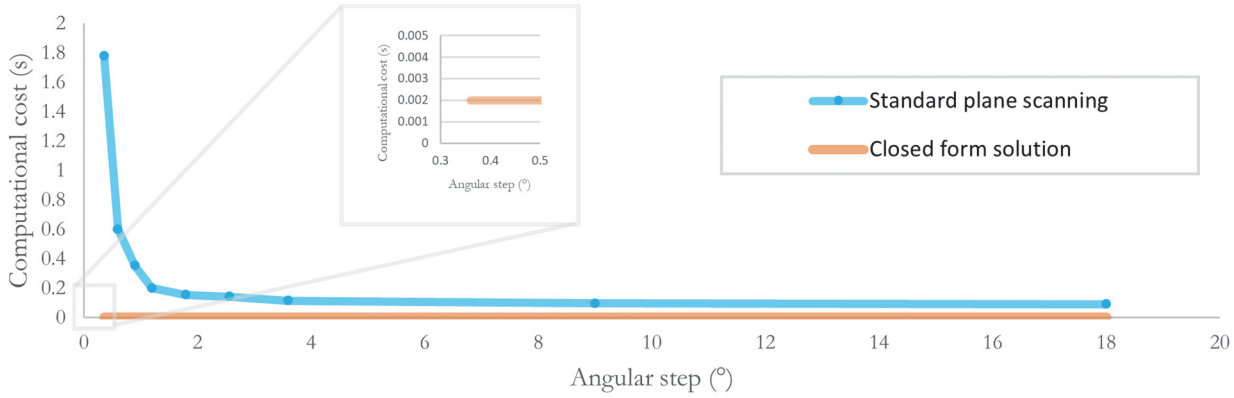

Figure 6: Comparison of computational cost between the standard scanning plane method and the closed form solution.

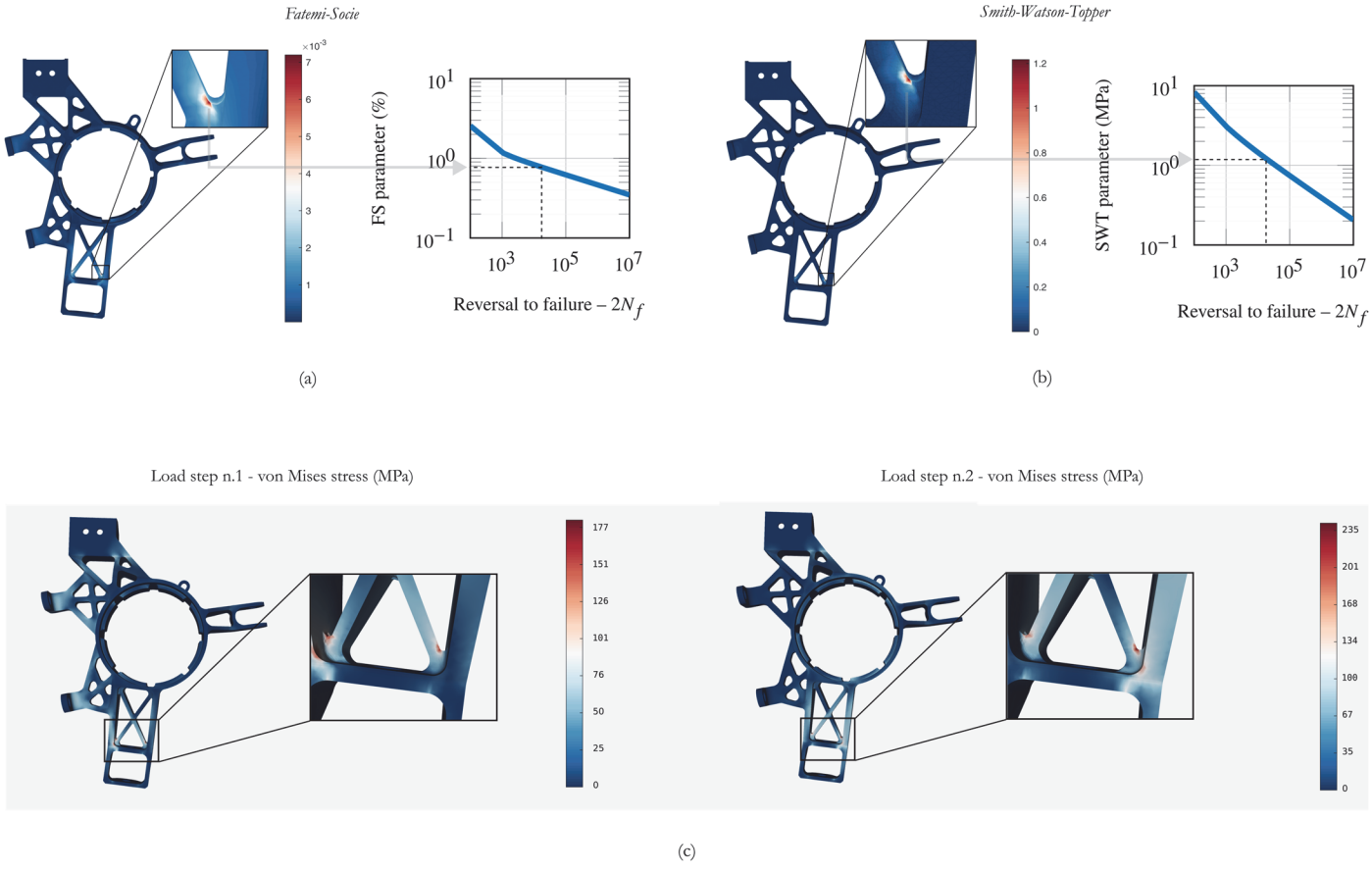

Figure 7: Critical plane factors' colour map for *Fatemi-Socie* (***FS***) (a) and *Smith-Watson-Topper* (***SWT***) (b) parameters (the efficient method and the plane scanning method gave the same results) together with CP vs reversal to failure fatigue curves; the colour map for the von Mises equivalent stress at the two load steps is provided as a comparison (c).

Fig. 7a-b illustrate the CP colour map for the upright component, showing the values of the *Fatemi-Socie* (***FS***) and *Smith-Watson-Topper* (***SWT***) critical plane factors according to both the efficient method and the standard plane scanning method; since the CP factor values resulting from the application of the two methods perfectly matched just one plot is provided. As a comparative basis, the von Mises equivalent stress has been reported in Fig. 7c for both load steps. It must be kept in mind that no direct comparison can be performed between the critical plane factors and von Mises stress, since the former are related to a load cycle, while von Mises stress refers to a single load step. However, it can be noted how the critical regions are indeed similar for all the parameters. Additionally, the von Mises equivalent stress is not well suited as a parameter for fatigue assessment. Especially in this case it cannot convey information on the degree of load non-proportionality, information that is embedded instead in the CP factors.
In all cases, however, the critical region of the component is located in the lower arm of the upright, where the load is transmitted from the wheel to the tie rod and rear lower arm. Furthermore, CP-life curves are provided for each method, based on Eqns. 2-3. Both the ***FS*** and ***SWT*** models yield comparable damage results, with a minimum fatigue endurance of 1.8×10^4 cycles, surpassing the requirement for the given application.

Conclusions

The present study introduced a rapid and precise approach for assessing fatigue loads in components with complex geometries under non-proportional loading conditions and elastic-plastic material properties. This methodology relies on a recently published closed-form solution for determining the critical plane orientation and critical plane factor, developed by the authors. To exemplify the method, an upright component of the FSAE car of the University of Pisa Formula Student team was chosen. The applied loading and constraints were derived from previous dynamic analyses conducted during the Formula Student competition in 2020. Considering the component complexity and the non-proportional loading condition, the investigation focused on assessing the damage across the entire component since identifying the critical region beforehand was challenging. Two critical plane methods, namely the *Fatemi-Socie* and *Smith-Watson-Topper* critical plane factors, were employed for the fatigue analysis. By utilizing the efficient calculation algorithm, a significant reduction in computational effort was achieved. The calculation time decreased from approximately 7.3 h using the standard plane scanning method to 63 s using the efficient method. Importantly, the accuracy of the results was not compromised, as the efficient method yielded analytically correct solutions for the implemented critical plane factors. The utilization of efficient algorithms for critical plane calculations opens new opportunities for employing these methods in various industries, enabling rapid analysis of complex models subjected to non-proportional fatigue loading conditions. This capability becomes particularly advantageous for complex geometries, such as those obtained through topological optimization, with the objective of mass reduction.

Acknowledgement

Financed by the European Union - NextGenerationEU (National Sustainable Mobility Center CN00000023, Italian Ministry of University and Research Decree n. 1033 - 17\ 06\ 2022, Spoke 11 - Innovative Materials & Lightweighting). The opinions expressed are those of the authors only and should not be considered as representative of the European Union or the European Commission's official position. Neither the European Union nor the European Commission can be held responsible for them.

References

[1] Cowles, B.A. (1989). High cycle fatigue in aircraft gas turbines—an industry perspective, Int. J. Fract., 80(2), pp. 147–163, DOI: 10.1007/BF00012667.
[2] Kaldellis, J.K., Zafirakis, D.P. (2012).Trends, prospects, and r&d directions in wind turbine technology. Comprehensive Renewable Energy, 2, pp. 671–724.
[3] Koyama, M., Zhang, Z., Wang, M., Ponge, D., Raabe, D., Tsuzaki, K., Noguchi, H., Tasan, C.C. (2017). Bone-like crack resistance in hierarchical metastable nanolaminate steels, Science (80-.)., 355(6329), pp. 1055–1057, DOI: 10.1126/science.aal2766.
[4] Xu, L., Wang, K., Yang, X., Su, Y., Yang, J., Liao, Y., Zhou, P., Su, Z. (2021). Model-driven fatigue crack characterization

and growth prediction: A two-step, 3-D fatigue damage modeling framework for structural health monitoring, Int. J. Mech. Sci., 195, pp. 106226, DOI: 10.1016/j.ijmecsci.2020.106226.
[5] Bhaumik, S.K., Sujata, M., Venkataswamy, M.A. (2008). Fatigue failure of aircraft components, Eng. Fail. Anal., 15(6), pp. 675–694, DOI: 10.1016/j.engfailanal.2007.10.001.
[6] Zhao, X., Jin, N., Liu, X., Shi, Z. (2022). Fatigue failure analysis of steel crane beams with variable-section supports, Eng. Fail. Anal., 136, pp. 106217, DOI: 10.1016/j.engfailanal.2022.106217.
[7] Frendo, F. (2013). Analysis of the catastrophic failure of a dockside crane jib, Eng. Fail. Anal., 31, pp. 394–411, DOI: 10.1016/j.engfailanal.2013.02.026.
[8] Kuncham, E., Sen, S., Kumar, P., Pathak, H. (2022). An online model-based fatigue life prediction approach using extended Kalman filter, Theor. Appl. Fract. Mech., 117, pp. 103143, DOI: 10.1016/j.tafmec.2021.103143.
[9] Sgamma, M., Chiocca, A., Bucchi, F., Frendo, F. (2023). Frequency analysis of random fatigue: Setup for an experimental study, Appl. Res., pp. e202200066, DOI: 10.1002/appl.202200066.
[10] Chiocca, A., Frendo, F., Aiello, F., Bertini, L. (2022). Influence of residual stresses on the fatigue life of welded joints. Numerical simulation and experimental tests, Int. J. Fatigue, 162, pp. 106901, DOI: 10.1016/j.ijfatigue.2022.106901.
[11] Chiocca, A., Tamburrino, F., Frendo, F., Paoli, A. (2022). Effects of coating on the fatigue endurance of FDM lattice structures, Procedia Struct. Integr., 42, pp. 799–805, DOI: 10.1016/j.prostr.2022.12.101.
[12] Chiocca, A., Frendo, F., Bertini, L. (2021).Residual stresses influence on the fatigue strength of structural components. Procedia Structural Integrity, 38, pp. 447–56.
[13] Chiocca, A., Frendo, F., Bertini, L. (2020). Experimental evaluation of relaxed strains in a pipe-to-plate welded joint by means of incremental cutting process, Procedia Struct. Integr., 28, pp. 2157–67, DOI: 10.1016/j.prostr.2020.11.043.
[14] Frendo, F., Marulo, G., Chiocca, A., Bertini, L. (2020). Fatigue life assessment of welded joints under sequences of bending and torsion loading blocks of different lengths, Fatigue Fract. Eng. Mater. Struct., 43(6), pp. 1290–304, DOI: 10.1111/ffe.13223.
[15] Chiocca, A., Frendo, F., Bertini, L. (2019). Evaluation of residual stresses in a tube-to-plate welded joint, MATEC Web Conf., 300, pp. 19005, DOI: 10.1051/matecconf/201930019005.
[16] Chiocca, A., Frendo, F., Bertini, L. (2021). Evaluation of residual stresses in a pipe-to-plate welded joint by means of uncoupled thermal-structural simulation and experimental tests, Int. J. Mech. Sci., 199, pp. 106401, DOI: 10.1016/j.ijmecsci.2021.106401.
[17] Meneghetti, G., Campagnolo, A., Visentin, A., Avalle, M., Benedetti, M., Bighelli, A., Castagnetti, D., Chiocca, A., Collini, L., De Agostinis, M., De Luca, A., Dragoni, E., Fini, S., Fontanari, V., Frendo, F., Greco, A., Marannano, G., Moroni, F., Pantano, A., Pirondi, A., Rebora, A., Scattina, A., Sepe, R., Spaggiari, A., Zuccarello, B. (2022). Rapid evaluation of notch stress intensity factors using the peak stress method with 3D tetrahedral finite element models: Comparison of commercial codes, Fatigue Fract. Eng. Mater. Struct., 45(4), pp. 1005–1034, DOI: 10.1111/ffe.13645.
[18] Fontana, F., Chiocca, A., Sgamma, M., Bucchi, F., Frendo, F. (2023). Numerical-experimental characterization of the dynamic behavior of PCB for the fatigue analysis of PCBa, Procedia Struct. Integr., 47, pp. 757–64, DOI: 10.1016/J.PROSTR.2023.07.043.
[19] Lazzarin, P., Berto, F. (2005). Some expressions for the strain energy in a finite volume surrounding the root of blunt V-notches, Int. J. Fract., 135(1–4), pp. 161–85, DOI: 10.1007/s10704-005-3943-6.
[20] Berto, F., Lazzarin, P., Radaj, D. (2009). Fictitious notch rounding concept applied to sharp V-notches: Evaluation of the microstructural support factor for different failure hypotheses. Part II: Microstructural support analysis, Eng. Fract. Mech., 76(9), pp. 1151–1175, DOI: 10.1016/j.engfracmech.2008.01.015.
[21] Mroziński, S. (2019). Energy-based method of fatigue damage cumulation, Int. J. Fatigue, 121, pp. 73–83, DOI: 10.1016/j.ijfatigue.2018.12.008.
[22] Varvani-Farahani, A., Haftchenari, H., Panbechi, M. (2007). An energy-based fatigue damage parameter for off-axis unidirectional FRP composites, Compos. Struct., 79(3), pp. 381–389, DOI: 10.1016/j.compstruct.2006.02.013.
[23] Braccesi, C., Morettini, G., Cianetti, F., Palmieri, M. (2018).Evaluation of fatigue damage with an energy criterion of simple implementation. Procedia Structural Integrity, 8, pp. 192–203.
[24] Morettini, G., Braccesi, C., Cianetti, F., Razavi, N. (2021). Design and implementation of new experimental multiaxial random fatigue tests on astm-a105 circular specimens, Int. J. Fatigue, 142, pp. 105983, DOI: 10.1016/j.ijfatigue.2020.105983.
[25] Morettini, G., Braccesi, C., Cianetti, F., Razavi, N., Solberg, K., Capponi, L. (2020). Collection of experimental data for multiaxial fatigue criteria verification, Fatigue Fract. Eng. Mater. Struct., 43(1), pp. 162–174, DOI: 10.1111/ffe.13101.
[26] Berto, F., Lazzarin, P. (2009).The volume-based strain energy density approach applied to static and fatigue strength assessments of notched and welded structures. Procedia Engineering, 1, pp. 155–158.

[27] Taylor, D., Barrett, N., Lucano, G. (2002). Some new methods for predicting fatigue in welded joints, Int. J. Fatigue, 24(5), pp. 509–518, DOI: 10.1016/S0142-1123(01)00174-8.
[28] Radaj, D., Sonsino, C.M., Fricke, W. (2006). Fatigue Assessment of Welded Joints by Local Approaches: Second Edition.
[29] Findley, W.N. (1959). A Theory for the Effect of Mean Stress on Fatigue of Metals Under Combined Torsion and Axial Load or Bending, J. Eng. Ind., 81(4), pp. 301–305, DOI: 10.1115/1.4008327.
[30] Socie, D. (1987). Multiaxial fatigue damage models, J. Eng. Mater. Technol. Trans. ASME, 109(4), pp. 293–298, DOI: 10.1115/1.3225980.
[31] Reis, L., Li, B., De Freitas, M. (2014). A multiaxial fatigue approach to Rolling Contact Fatigue in railways, Int. J. Fatigue, 67, pp. 191–202, DOI: 10.1016/j.ijfatigue.2014.02.001.
[32] El-sayed, H.M., Lotfy, M., El-din Zohny, H.N., Riad, H.S. (2018). Prediction of fatigue crack initiation life in railheads using finite element analysis, Ain Shams Eng. J., 9(4), pp. 2329–2342, DOI: 10.1016/j.asej.2017.06.003.
[33] Zhu, S.P., Yu, Z.Y., Correia, J., De Jesus, A., Berto, F. (2018). Evaluation and comparison of critical plane criteria for multiaxial fatigue analysis of ductile and brittle materials, Int. J. Fatigue, 112, pp. 279–288, DOI: 10.1016/j.ijfatigue.2018.03.028.
[34] Cruces, A.S., Garcia-Gonzalez, A., Moreno, B., Itoh, T., Lopez-Crespo, P. (2022). Critical plane based method for multiaxial fatigue analysis of 316 stainless steel, Theor. Appl. Fract. Mech., 118, pp. 103273, DOI: 10.1016/j.tafmec.2022.103273.
[35] Chiocca, A., Frendo, F., Marulo, G. (2023). An efficient algorithm for critical plane factors evaluation, Int. J. Mech. Sci., 242, pp. 107974, DOI: 10.1016/j.ijmecsci.2022.107974.
[36] Chiocca, A., Sgamma, M., Frendo, F. (2023). Closed-form solution for the Fatemi-Socie extended parameter in case of linear elasticity and proportional loading, Fatigue Fract. Eng. Mater. Struct., DOI: 10.1111/FFE.14153.
[37] Marques, J.M.E., Benasciutti, D., Carpinteri, A., Spagnoli, A. (2020). An algorithm for fast critical plane search in computer-aided engineering durability analysis under multiaxial random loadings: Application to the Carpinteri–Spagnoli–Vantadori spectral method, Fatigue Fract. Eng. Mater. Struct., 43(9), pp. 1978–1993, DOI: 10.1111/ffe.13273.
[38] Wentingmann, M., Noever-Castelos, P., Balzani, C. (2020).An adaptive algorithm to accelerate the critical plane identification for multiaxial fatigue criteria. Proceedings of the 6th European Conference on Computational Mechanics: Solids, Structures and Coupled Problems, ECCM 2018 and 7th European Conference on Computational Fluid Dynamics, ECFD 2018, pp. 3745–3754.
[39] Sunde, S.L., Berto, F., Haugen, B. (2020). Efficient implementation of critical plane for 3D stress histories using triangular elements, Int. J. Fatigue, 134, pp. 105448, DOI: 10.1016/j.ijfatigue.2019.105448.
[40] Fatemi, A., Socie, D.F. (1988). A critical plane approach to multiaxial fatigue damage including out-of-phase loading, Fatigue Fract. Eng. Mater. Struct., 11(3), pp. 149–165, DOI: 10.1111/j.1460-2695.1988.tb01169.x.
[41] Gates, N.R., Fatemi, A. (2017). On the consideration of normal and shear stress interaction in multiaxial fatigue damage analysis, Int. J. Fatigue, 100, pp. 322–336, DOI: 10.1016/j.ijfatigue.2017.03.042.